



# An assessment of the spatio-temporal dynamics of Landsat-derived aerosol concentration in relation with land cover and road networks in the Lagos megacity

Emmanuel Ayodele<sup>1</sup> · Chukwuma Okolie<sup>1,2</sup> · Samuel Akinnusi<sup>1</sup> · Erom Mbu-Ogar<sup>1</sup> · Rose Alani<sup>2,3</sup> · Olagoke Daramola<sup>1</sup> · Abdulwaheed Tella<sup>2,4,5,6</sup>

Received: 29 June 2022 / Accepted: 24 December 2022 / Published online: 18 January 2023  
© The Author(s), under exclusive licence to Springer-Verlag GmbH Germany, part of Springer Nature 2023

## Abstract

The interrelationships between air quality, land cover change, and road networks in the Lagos megacity have not been explored. Globally, there are knowledge gaps in understanding these dynamics, especially using remote sensing data. This study used multi-temporal and multi-spectral Landsat imageries at four epochs (2002, 2013, 2015, and 2020) to evaluate the aerosol optical thickness (AOT) levels in relation to land cover and road networks in the Lagos megacity. A look-up table (LUT) was generated using Py6S, a python-based 6S module, to simulate the AOT using land surface reflectance and top of atmosphere reflectance. A comparative assessment of the method against in situ measurements of particulate matter (PM) at different locations shows a strong positive correlation between the imagery-derived AOT values and the PMs. The AOT concentration across the land cover and road networks showed an increasing trend from 2002 to 2020, which could be explained by urbanization in the megacity. The higher concentration of AOT along the major roads is attributed to the high air pollutants released from vehicles, including home/office generators and industries along the road corridors. The continuous rise in pollutant values requires urgent intervention and mitigation efforts. Remote sensing-based AOT monitoring is a possible solution.

**Keywords** Air quality · Aerosol optical thickness · Particulate matter · Lagos megacity · Land cover · Road networks

## Introduction

Responsible Editor: Philippe Garrigues

✉ Samuel Akinnusi  
akinnusisamuel1845@gmail.com

<sup>1</sup> Department of Surveying and Geoinformatics, Faculty of Engineering, University of Lagos, Lagos, Nigeria

<sup>2</sup> Air Quality Monitoring (AQM) Research Group, University of Lagos, Lagos, Nigeria

<sup>3</sup> Department of Chemistry, Faculty of Science, University of Lagos, Lagos, Nigeria

<sup>4</sup> Department of Civil and Environmental Engineering, Geospatial Analysis and Modelling (GAM) Research Laboratory, Universiti Teknologi PETRONAS (UTP), Seri Iskandar, Perak, Malaysia

<sup>5</sup> Division of Earth, Environment and Space, Foresight Institute of Research and Translation, Ibadan, Nigeria

<sup>6</sup> Division of Environment and Sustainability, The Hong Kong University of Science and Technology, Clear Water Bay, Hong Kong SAR, China

Air pollution affects over 90% of the world's population, resulting in an estimated seven million deaths annually. This makes it one of the world's largest environmental health problems and global health risks. Air pollution sources with adverse impacts on air quality are mostly found in urban areas due to rapid population growth and urbanization (Taiwo et al. 2015; Njoku et al. 2016; Joshi et al. 2019). There is an increase in the discharge of pollutants into the air, water, and soil from transportation sources, growing energy consumption, and waste production due to lack of strict implementation of environmental regulations in urban areas (Prakash et al. 2016). Urban air pollution in Nigeria has increased rapidly due to the aforementioned problems. According to the World Health Organization (WHO) report of 2016, Nigeria has a mortality rate of 0.3% attributed to air pollution, the second-worst in all of Africa. The report revealed that more people die from air pollution in Nigeria than in South Africa, Kenya, and Angola combined. One

primary source of air pollution in Nigeria is atmospheric aerosols, which must be taken seriously.

Atmospheric aerosols consist of solid and liquid microscopic particles and gas carriers and are a poly-disperse system suspended in the atmosphere with particle sizes ranging between  $10^{-3}$   $\mu\text{m}$  and  $10^2$   $\mu\text{m}$  (Yang et al. 2017). Aerosols can be classified into three categories based on particle size: ultrafine particles, fine particles, and coarse particles. Ultrafine particles are a particulate matter of sizes between 0.001 and 0.2  $\mu\text{m}$  in diameter, fine particles range between 0.2 and 2.0  $\mu\text{m}$  in diameter, while coarse particles include particles beyond 2.0  $\mu\text{m}$  in diameter. Interactions between aerosols and solar radiation through the dispersion and absorption processes have a major effect on the planet's radiative budget and they create substantial uncertainties in global climate models (Omari et al. 2019). Therefore, regular measurements of their optical properties, such as AOT, are needed to track the high temporal and spatial variability of aerosol concentrations, one of the major causes of attenuation in the atmosphere (Omari et al. 2019). According to Zhang et al. (2014), AOT is a typical atmospheric monitoring measure of aerosols. AOT is defined as an integrated coefficient of extinction over a vertical column of a specific cross section in which the coefficient of extinction is the fractional radiance depletion per length of the path (Yang et al. 2017; Omari et al. 2019). In other words, the AOT represents the degree of aerosol-weakened solar radiation that can indirectly reflect the concentration of aerosols and the degree of regional atmospheric pollution. Ground-based sun photometers and satellite sensors are the two primary approaches for monitoring aerosols (Wei et al. 2020).

Ground-based platforms can provide more accurate near-real-time AOT data for a small area. However, satellite remote sensing technologies have facilitated dynamic real-time aerosol monitoring globally, even in inaccessible regions where the conventional ground methods are limited, which is the case in most countries (Sun et al. 2016; Wei et al. 2020). Meanwhile, satellite monitoring systems play vital roles in the broad-level or macro-scale derivation of spatial data (Ranjan et al. 2020). Compared to the ground-based technique of aerosol monitoring, remote sensing and geographic information systems (GIS) offer a cost-effective and timely approach to atmospheric aerosols monitoring. Moreover, the spatial variability of AOT can be examined much better from satellite sensors. As a result, some scientists have adopted the satellite-based method of air quality mapping of various geographical areas, especially in urban centers (Ou et al. 2017; Omari et al. 2019; Liu et al. 2020).

Several models and algorithms have been developed by researchers based on radiation transfer to correct the effects of atmospheric attenuations and to estimate the concentration of aerosols. Notable radiative transfer codes or models for simulating atmospheric radiation include 6S/6SV (Vermote et al. 1997), libRadtran (Mayer and Kylling. 2005), and LOWTRAN

(Ding et al. 2015). The simulated radiation is further used for atmospheric correction to determine atmospheric aerosol and other atmospheric constituents affecting radiation transfer. These are physically dependent calibration models, which are very complex and require several input parameters acquired during remote sensing data acquisition from the in situ field atmospheric information (Ding et al. 2015). Based on radiative transfer equations, there are several methods that different researchers have developed to estimate AOT. Some of the common methods include the structure-function method, multi-angle polarization method, contrast reduction method (Tanre et al. 1979), Deep Blue (DB) algorithm, Dark Target (DT) algorithm or densely dark vegetation (DDV) method (Kaufman et al. 1988; Kaufman et al. 1997), and improved DT method (Levy et al. 2007; Yang et al. 2017). In general, the difficulties in satellite AOT retrieval are related to the removal of surface reflectance, clouds, and the selection of an appropriate aerosol model (Omari et al. 2019). Herman et al. (1997) and Deuzé et al. (2001) introduced the multi-angle polarization method to remove reflectance due to polarization and directionality of the earth's reflectances (polarization and anisotropy of reflectances and this accounts for an anisotropic effect). The structure-function method was introduced by Holben et al. (1998) for inverting AOT from total atmospheric transmittance. The DT algorithm is ideal for vegetated/dark-soiled ground, in which the surface reflectance at two visible channels can be parameterized based on the dynamic relationship between blue and red channels and short-wave infrared channel (Kaufman et al. 1997; Levy et al. 2007; Tian et al. 2018). This is essential to account for all the sources that can influence the results such as the land cover change and vehicular traffic. For example, land cover change can influence the concentration of pollutants in the environment when natural land cover is replaced with anthropogenic sources of pollution.

Lagos State, the fastest-growing urban center in Nigeria, has been experiencing air pollution problems in all their severity over the past decades; this is associated with a high density of industries, transport networks, and open waste burning (Njoku et al. 2016). An increase in technological, industrial, and agricultural advancement, coupled with the rise in population growth, has triggered the deterioration of environmental air quality in Lagos State (Oluyemi and Asubiojo. 2001; Njoku et al. 2016). In Lagos, the socio-economic conditions, traffic density, proximity to emission sources, and access to healthcare create a differential susceptibility to ill health attributable to air pollution (Olowoporoku et al. 2012). Daily, more than eight million people, moving in five million vehicles, cram into a very small network of roads (CNN Travel. 2019). Lagos State has been recognized as one of the world's megacities undergoing rapid urbanization and urban sprawl (Obiefuna et al. 2013).

Several studies have examined the concentration and spatial distribution of air pollutants in Lagos State (Oluyemi

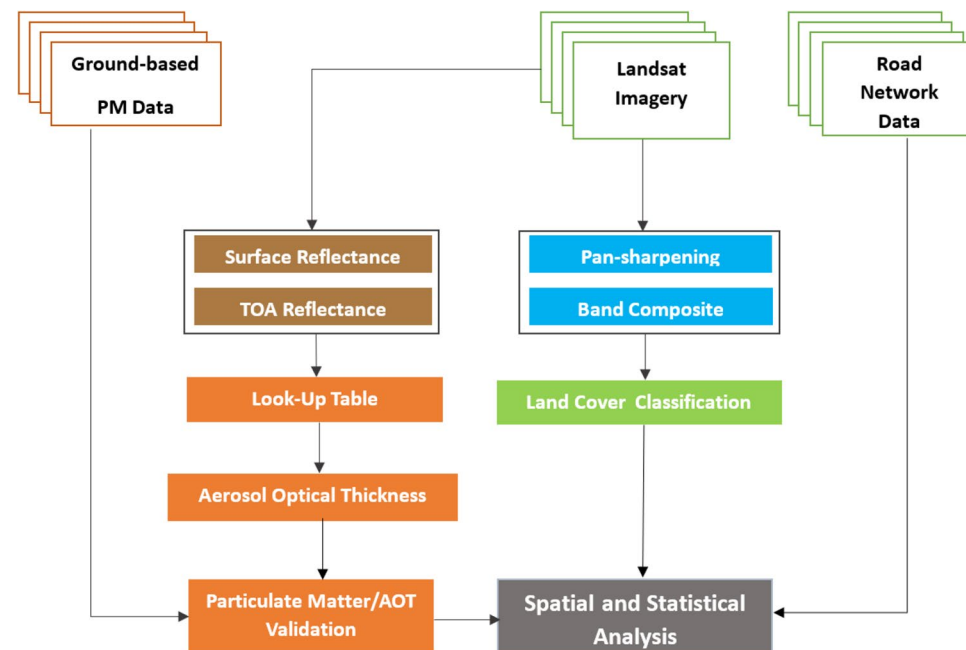
and Asubiojo. 2001; Adeyewa et al. 2011; Oguntunde et al. 2014; Alani et al. 2019). However, there are still some knowledge gaps in understanding atmospheric aerosol concentration, not only in Lagos State but in Africa and the world. Secondly, the existing literature has not showcased a holistic perspective on air pollution dynamics and its relationship with land cover change and road network distribution, which would be instrumental for a futuristic outlook of air quality in the state. Several studies have established the variations at selected locations in Lagos using ground-based sensor techniques. However, there is limited information on the state-wide pattern of aerosol concentration and its variability in areas not covered by ground monitoring stations. Also, most earlier studies were limited to ground-based data captured at specific periods without considering the long-term temporal variations. From a holistic perspective, this study assesses the spatio-temporal dynamics of aerosol concentration in the Lagos megacity, specifically within 17 local government areas (LGAs).

## Methodology

### Materials and methods

The methodology adopted in this study incorporates spatial modelling and analysis, which have been identified by Tella et al. (2021) as essential procedures in decision-making processes of mitigating poor air quality. Figure 1 presents the workflow diagram, while the stages are discussed in the following sections.

**Fig. 1** The workflow diagram of the methodology



### Study area

Figure 2 presents the map of the study area showing the 17 local government areas (LGAs) under study that include Agege, Alimosho, Amuwo-Odofin, Apapa, Eti-Osa, Lagos Mainland, Ikeja, and Ikorodu. The choice of Lagos State is necessitated by the concentration of commercial, industrial, and educational activities, consequently resulting in urbanization, overpopulation, and traffic congestion. Lagos State accounts for about 30% of all traffic in Nigeria (Car Mart. 2022), which is a big challenge given the limited road infrastructure and development. Also, 70% of Nigeria's industrial and commercial activities are in the Lagos region, making it the commercial nerve center and the most populous state in the country (Yusuf et al. 2013). According to Faisal et al. (2021), the population of Lagos city is increasing ten times faster than New York and Los Angeles. The study area is also ideal for examining the seasonal variations due to climatic changes, such as the rainy season (April–October) and the dry season (November–March), and how they might affect pollutants dispersion and concentration. Accordingly, the importance of this research, using Lagos State as a case study, cannot be over-emphasized.

### Data acquisition

#### Landsat imagery

Landsat 7 Enhanced Thematic Mapper (ETM+) and Landsat 8 Operational Land Imager (OLI) satellite imageries were downloaded from the online archive of the United States Geological Survey-USGS (<https://earthexplorer.usgs.gov/>).



**Fig. 2** Map of the study area in the Lagos megacity

**Table 1** Characteristics of the Landsat imageries

Dataset	Acquisition date (yyyy-mm-dd)	Acquisition time (GMT)
Landsat 7 ETM+	2002-12-28	09:51:41
Landsat 8 OLI	2013-12-18	10:04:25
	2015-12-08	10:03:03
	2020-01-20	10:03:05

As an improvement on the previous Landsat missions, Landsat 8 OLI has additional spectral bands (coastal and cirrus), radiometric solution enhancements from 8 to 12 bits (16 bits when processed into Level-1 data products), upgraded signal to noise ratio (SNR), and the spectral response functions particularly the near-infrared band. The selection criteria for the imageries were predicated on the absence of cloud cover or its minimal presence. This placed the acquisition dates of the imageries within the dry season months of January and December, which have lower humidity, rainfall, and cloud presence than the rainy season. Table 1 shows the characteristics of the selected Landsat imageries.

#### Particulate matter (PM) data

Particulate matter ( $PM_{1.0}$ ,  $PM_{2.5}$ , and  $PM_{10}$ ) data were obtained using the ground-based Air Quality Egg instrument. The Egg is a WiFi-enabled system that tracks changes in the levels of specified air pollutants using sensors. Figure 3 presents the Air Quality Egg instrument used in this



**Fig. 3** Ground-based measurement of PM at Onike with the Air Quality Egg

study. This sensor allows users to gather very high-resolution measurements of gaseous and particle pollutants. Specifically, the Air Quality Egg carries an optical particulate sensor that can quantify particles between 0.5 and 10  $\mu\text{m}$  in size range, such as pollen, spored, dust mites, smog, cigarette smoke, dust settling, and ambient dust. It was used to determine the concentration levels of  $PM_{1.0}$ ,  $PM_{2.5}$ , and  $PM_{10}$  at different sites of interest within the megacity. At the selected sites (Onike and Okobaba, shown in Fig. 4), the sensing system in the device was installed on the wall of different platforms and communicated wirelessly to the egg-shaped base station inside, which transmitted the data to the Internet. The acquired PM data were retrieved from the air quality website using the Egg serial number and claim

**Fig. 4** Map of selected PM monitoring sites



code. Also, some data were recorded manually on-site from the displayed readings on the Air Quality Egg. The data were measured weekly between 9:00 a.m. and 5:00 p.m. from February 2019 to July 2019 for different locations within Onike and Okobaba communities.

### Road networks data

The daily commute in Lagos megacity is through road, water, rail, and air, while road travel is the most prevalent and extensively used (Mogaji 2020). As a result, the pollution from vehicle exhausts has immensely contributed to the deteriorating air quality in the state. Therefore, examining the concentration of AOT along the road networks is worthwhile. The road network data is readily available on the OpenStreetMap platform and was downloaded for free. The data was downloaded with the BBBIKE web-based tool (<https://extract.bbbike.org/>) from the OpenStreetMap archive. The downloaded road layer is in different road categories including expressway, main road, minor road, and street. The road types used for this study are the expressway and main road.

### Data processing

#### AOT retrieval model

The major difficulty in retrieving aerosols from satellite imagery is the separation of atmospheric radiance and land

surface radiance from the total radiance recorded by the sensor (Zhang et al. 2015; Sun et al. 2016; Omari et al. 2019). The method of AOT retrieval, which is based on dark target pixel, is known as the dense dark vegetation (DDV) method. This method is based on good correlation between the blue (470 nm), red (660 nm), and shortwave infrared (2100 nm) spectral bands (Omari et al. 2019; Tian et al. 2018). Once the dark target has been identified, its reflectance can be derived through atmospheric correction, where the true surface reflectance will be determined. Then atmospheric aerosol can be retrieved from the relationship between the surface reflectance, top of atmosphere (ToA) reflectance or apparent reflectance, and atmospheric reflectance using a LUT (Omari et al. 2019; Ou et al. 2017; Sun et al. 2016). AOT derived with LUTs has some inherent limitations. Firstly, a specific aerosol model is used to generate the LUT, but it needs to be recalculated each time the aerosol model is modified. Secondly, the final outcome may be impacted by the LUT size. No viable LUT size with suitable angle or AOD intervals has been established yet. For the direct calculation of satellite AOT, some researchers have created modified RTMs that use single-scattering for the atmospheric reflectance approximation to deal with the drawbacks of the LUT technique. Therefore, this study used the second simulation of the satellite signal in the solar spectrum, which uses single-scattering for deriving atmospheric reflectance, to generate AOT. In the following sections, the process of estimating the surface reflectance from satellite imagery is explained, including using the 6S model for determining AOT.

## Land surface reflectance determination

The DDV technique was adopted in this study to estimate the land surface reflectance. This was done using the improved dark-pixel method developed by Levy et al. (2010), which is dependent on Normalized Difference Vegetation Index (NDVI) and scattering angle. The equations for determining the surface reflectance of Landsat 8 OLI and Landsat 7 ETM+ are given by Luo et al. (2015), Ou et al. (2017), and Okolie et al. (2021). The calculation was done using the ArcGIS Raster calculator.

Calculating the surface reflectance using Landsat 8 OLI and Landsat 7 ETM+;

$$\rho_{s(0.66)} = f(\rho_{s(2.1)}) = \rho_{s(2.1)} \times \text{slope}_{0.66/2.1} + \text{yint}_{0.66/2.1} \quad (1)$$

$$\text{slope}_{0.66/2.1} = \text{slope}_{0.66/2.1}^{\text{NDVI}_\text{SWIR}} + 0.002 \times \Theta - 0.27 \quad (2)$$

$$\text{yint}_{0.66/2.1} = -0.00025\Theta + 0.033 \quad (3)$$

$$\begin{aligned} \text{slope}_{0.66/2.1}^{\text{NDVI}_\text{SWIR}} &= 0.48 & (\text{NDVI}_\text{SWIR} < 0.25) \\ \text{slope}_{0.66/2.1}^{\text{NDVI}_\text{SWIR}} &= 0.58 & (\text{NDVI}_\text{SWIR} > 0.75) \\ \text{slope}_{0.66/2.1}^{\text{NDVI}_\text{SWIR}} &= 0.48 + 0.2 \times (\text{NDVI}_\text{SWIR} - 0.25) & (\text{NDVI}_\text{SWIR} < 0.25) \end{aligned}$$

Calculating the vegetation index;

$$\text{NDVI}_\text{SWIR} = \frac{\rho_{\text{TOA}(1.6)} - \rho_{\text{TOA}(2.1)}}{\rho_{\text{TOA}(1.6)} + \rho_{\text{TOA}(2.1)}} \quad (4)$$

$$\Theta = \cos^{-1}(\cos \theta \cos \theta_0 + \sin \theta \sin \theta_0 \cos(\Delta\varphi)) \quad (5)$$

where

$\rho_{s(0.66)}$ = red-band surface reflectance  
 $\rho_{s(2.1)}$ = apparent reflectance, SWIR 2 (Band 7: Landsat 8; and Band 7: Landsat 7)

$\rho_{\text{TOA}(1.6)}$ = apparent reflectance SWIR 1 (Band 6: Landsat 8; and Band 5: Landsat 7)

$\rho_{\text{TOA}(2.1)}$ = apparent reflectance SWIR 2 (Band 7: Landsat 8; and Band 7: Landsat 7)

$\Theta$  = scattering angle

$\theta$  = sensor zenith angle

$\theta_0$  = solar zenith angle

$\Delta\varphi$  = relative azimuth angle

$\text{NDVI}_\text{SWIR}$  = Normalized Difference Vegetation Index

## Constructing the look-up table (LUT)

The 6S radiation transfer model has been used in the Earth-atmosphere system to simulate the transmission of solar radiation, and it is a commonly accepted and applied model (Vermote et al. 1997; Zhao et al. 2016). 6S is used operationally as part of the atmospheric correction procedure for Landsat, and a variety of sensors. Py6S is a Python interface to the 6S model. In this study, the 6S model was run on the Python interface to simulate the atmospheric properties of the Landsat 8 OLI and Landsat 7 ETM sensor for blue and red bands (Wilson 2013). Table 2 and Fig. 5 show the input parameters in the python script within the Jupyter notebook environment used for the generation of the LUT.

## Image classification

Pan sharpening and generation of band composites was done within the ENVI software environment. ENVI is a remote sensing software for image processing, analysis, and extracting information from geospatial imagery(L3Harris Geospatial 2021). Band composites were generated from the Landsat imageries using different band combinations to aid the image classification process as different band combinations emphasize different land cover features differently. Next, the region of interest (ROI) tool within ENVI was used to select training classes representing each land cover feature. Using the parallelepiped classification

**Table 2** LUT input parameters

Parameter	Input type	Input values
Atmospheric profiles	Tropical	-
Aerosol profiles	Continental	-
Ground reflectance	Homogeneous Lambertian	-
Geometry	User	-
	Solar zenith	37.9
	Solar azimuth	142.77
	Sensor view zenith	0
	Sensor view azimuth	0
	Month	12
	Day	8
	Decimal hour	10.05
Altitudes	Custom altitude	0.04
	Sensor satellite level	-
Wavelengths	Landsat OLI Band 4	-
Atmospheric corrections	Lambertian reflectance	-
Aerosol at 550 nm	AOT	-

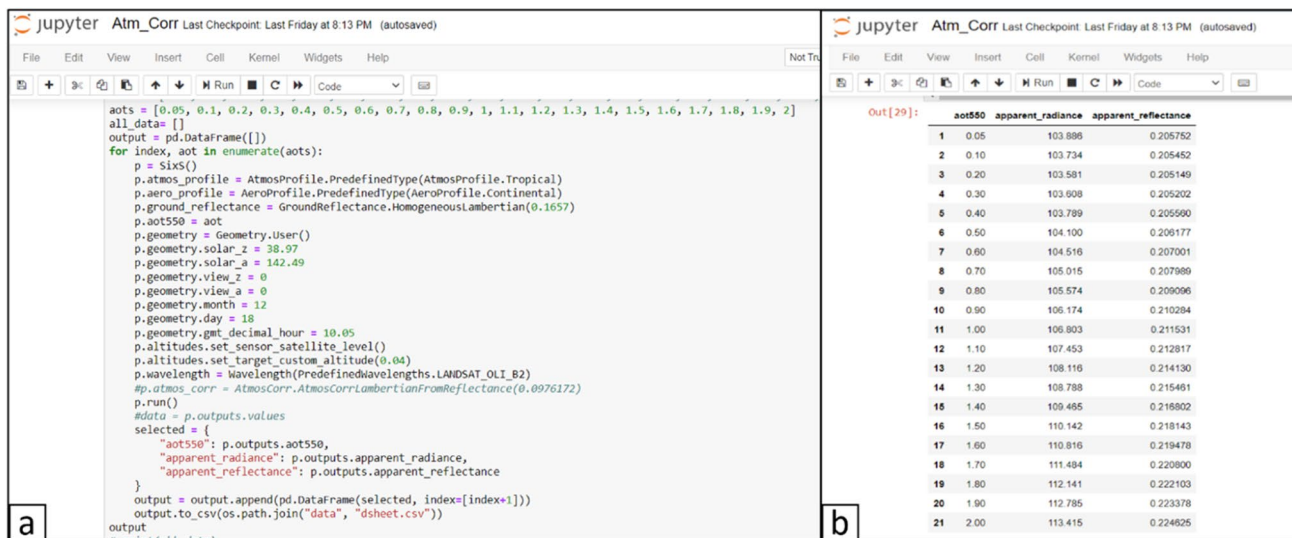


**Fig. 5** (a) Input parameters for the Py6S. (b) Output look-up table

**Table 3** Accuracy assessment of image classification

Year	Overall accuracy	Kappa coefficient
2002	0.881	0.823
2013	0.908	0.893
2020	0.962	0.932

algorithm, the Landsat imageries were then classified into five information classes—bare land, built-up area, vegetation, water body, and wetland. This image processing operation was carried out within the ENVI Classic v 5.0 software environment. The different classes identified in ENVI were processed and saved to shapefile to produce the map in ArcGIS software.

### Accuracy assessment for image classification

Accuracy assessment was used to determine the classification accuracy of land cover data. The accuracy required to classify different types of land cover using remotely sensed imagery must be at least 85% for the accuracy assessment exercise (Anderson, 1971; Alademomi et al. 2020). An accuracy evaluation was performed by comparing the interpreted features on the imagery and their related classification outputs using 250 random sample points. Overall accuracy and the kappa coefficient were computed. (see Table 3). The kappa coefficient and overall accuracy of classification were calculated with the following formulae (Das and Angadi, 2020).

$$K = \frac{N \sum_{i=1}^r X_{ii} - \sum_{i=1}^r (x_{i+} \times x_{+i})}{N^2 - \sum_{i=1}^r (x_{i+} \times X_{+i})} \quad (6)$$

where

$r$  = number of rows and columns in error matrix

$N$  = total number of observations (pixels)

$X_{ii}$  = observation in row  $i$  and column  $i$

$x_{i+}$  = marginal total of row  $i$

$x_{+i}$  = marginal total of column  $i$

$K$  = Kappa coefficient

$$\text{Overall accuracy} = \frac{\text{Total number of correct samples}}{\text{Total number of samples}} \times 100 \quad (7)$$

It was noted that 2020 had the highest accuracy than the previous years. This may be due to the improvement in the Landsat 8 OLI sensor over the Landsat 7 ETM sensor.

### Quantitative analysis and validation

The quantitative analysis enabled an understanding of the values associated with spatial and temporal changes. Descriptive statistics such as the minimum, maximum,

mean, and standard deviations were used to summarize the data for interpretation. The “Zonal Statistics as Table” tool in ArcMap was used to summarize the values of the AOT in each LGA zone in a table. For validation, Pearson’s correlation coefficient was used to infer the level of interdependence between imagery-based AOT and the ground-based PM data.

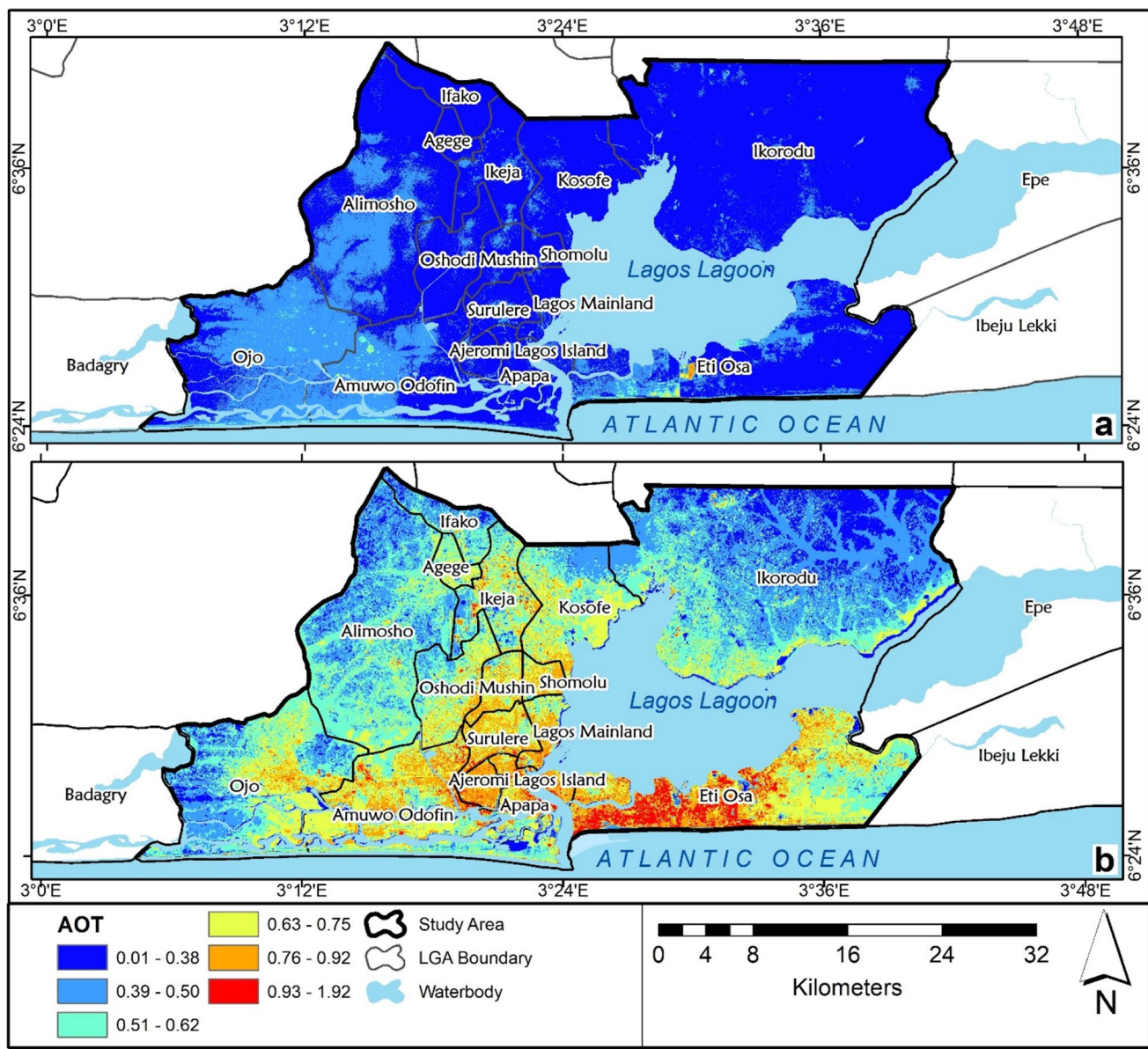
## Results and analysis

This section presents the Landsat-derived AOT maps, land cover maps for 2002, 2013, and 2020, and road network maps for 2002, 2013, 2015, and 2020 respectively, the

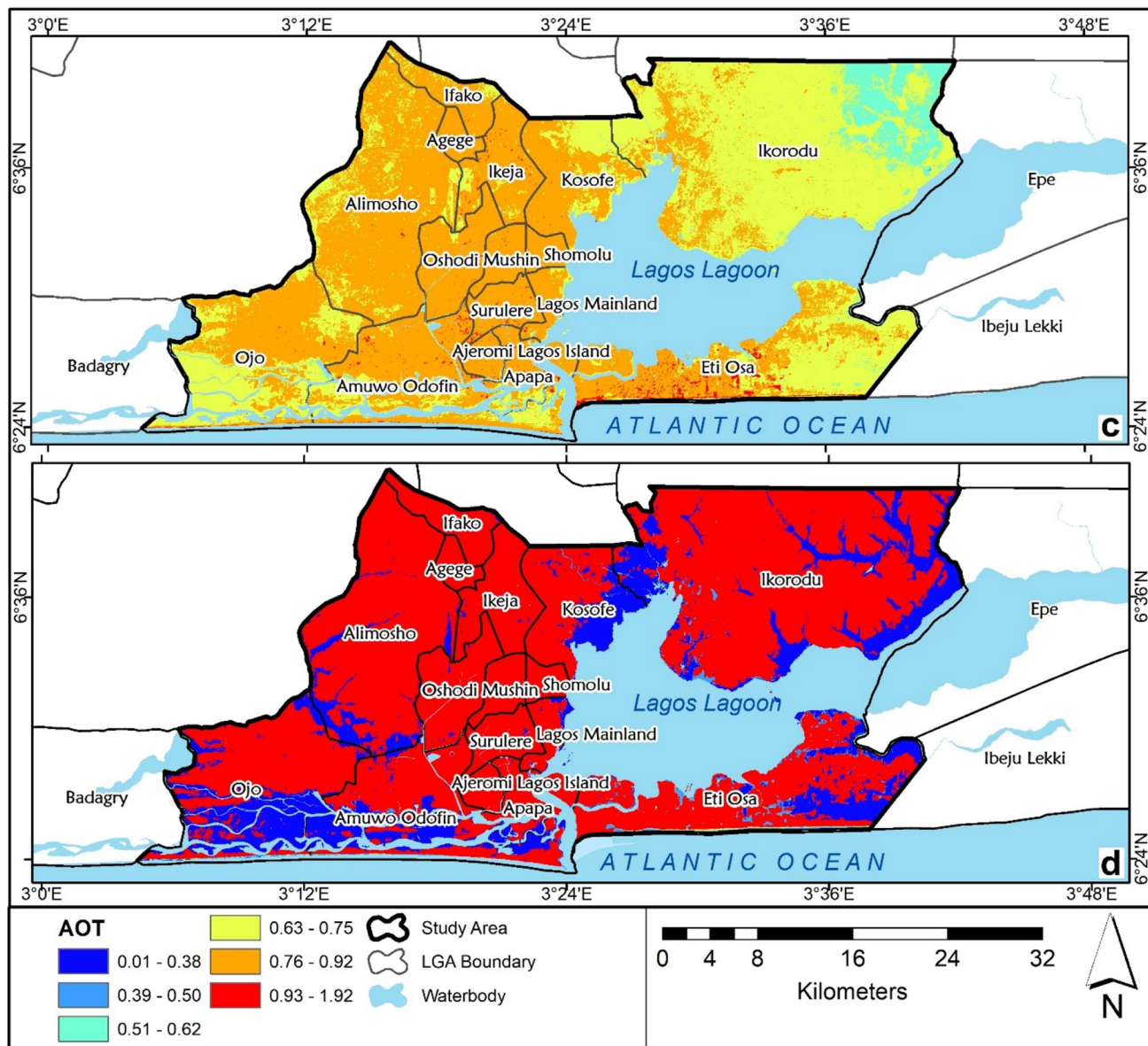
spatio-temporal and correlation analysis, and the validation with ground-based PM data.

### Analysis of AOT variation

Figure 6 (a), (b), (c), and (d) present the spatial distribution of AOT for 2002, 2013, 2015, and 2020 respectively. The AOT values over the study area were lowest in 2002, ranging from 0.052 to 0.976. In subsequent years, the AOT ranges were as follows: 0.008–1.920 (2013), 0.487–1.749 (2015), and 0.359–1.751 (2020). In 2002, the AOT values were generally higher in the following LGAs: Eti-Osa, Amuwo-Odofin, and Ojo, while the highest concentration levels were observed at the center of Eti-Osa LGA. In 2013, the AOT value was generally



**Fig. 6** Variation in AOT. (a) 2002. (b) 2013. (c) 2015. (d) 2020

**Fig. 6** (continued)

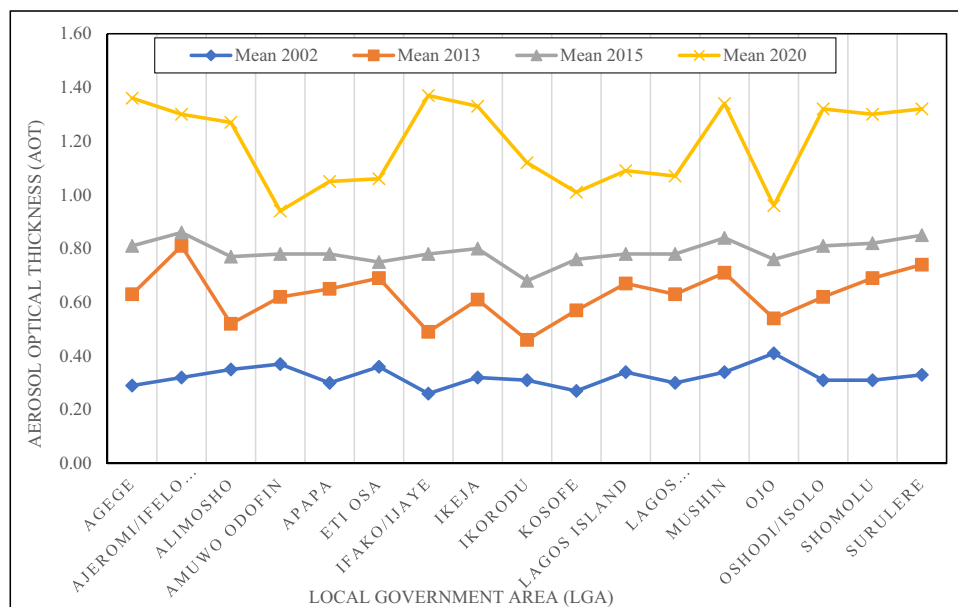
higher than in 2002, with the highest concentration observed in Eti-Osa (the south-eastern part of the megacity). Higher values were also observed in the central and northern parts of the megacity, including Mushin, Oshodi, Shomolu, Ikeja, Apapa, Ajeromi-Ife, Kosofe, Mainland, and Lagos Island.

In 2015, the AOT value was higher than in 2013. This is similar to the distribution observed in 2002 and 2013, with a very high AOT concentration observed in the central and south-eastern regions. Unlike the previous years, AOT concentration in 2020 was highest in the north-western part of the study area. Also, the concentration was high in the north-eastern and south-eastern regions, Ikorodu and Eti-Osa respectively, and in the center of the megacity in 2020.

Table 4 shows the minimum, maximum, and mean values of the AOT in the Lagos megacity for the study periods, while Fig. 7 illustrates the mean distribution. The zonal analysis involves the descriptive analysis of the spatial distribution of the AOT per LGA. In 2002, it is observed that the mean AOT ranges between 0.26 and 0.41, with the highest in Ojo and lowest in Ifako/Ijaye LGA. Ojo, Amuwo Odofin, and Eti-Osa recorded the highest mean AOT values of 0.41, 0.37, and 0.36, respectively in 2002. In Table 4, Ikorodu and Ajeromi-Ife had the lowest and highest recorded mean AOT values in 2013. Mushin and Surulere also had very high mean AOT values of 0.71 and 0.74, respectively, in 2013. In 2015, similar to 2013, the mean AOT values are

**Table 4** Minimum and maximum AOT per LGA, 2002–2020

LGA	Area (km <sup>2</sup> )	2002			2013			2015			2020		
		Min	Max	Mean									
Agege	11.09	0.12	0.46	0.29	0.14	1.72	0.63	0.68	1.03	0.81	1.21	1.57	1.36
Ajeromi/Ifeodun	12.23	0.17	0.55	0.32	0.22	1.74	0.81	0.68	1.07	0.86	0.50	1.67	1.30
Alimosho	183.56	0.12	0.64	0.35	0.12	1.35	0.52	0.65	1.09	0.77	0.44	1.57	1.27
Amuwo Odofin	133.35	0.18	0.79	0.37	0.16	1.83	0.62	0.55	1.36	0.78	0.41	1.64	0.94
Apapa	26.43	0.11	0.76	0.30	0.16	1.60	0.65	0.56	1.11	0.78	0.50	1.68	1.05
Eti-Osa	190.85	0.18	0.98	0.36	0.06	1.92	0.69	0.51	1.68	0.75	0.38	1.75	1.06
Ifako/Ijaye	26.40	0.09	0.67	0.26	0.11	1.83	0.49	0.65	1.00	0.78	0.48	1.56	1.37
Ikeja	45.78	0.10	0.88	0.32	0.14	1.90	0.61	0.65	1.75	0.80	0.46	1.67	1.33
Ikorodu	390.91	0.05	0.88	0.31	0.01	1.41	0.46	0.49	1.05	0.68	0.40	1.67	1.12
Kosofe	80.78	0.09	0.56	0.27	0.09	1.79	0.57	0.53	1.13	0.76	0.46	1.67	1.01
Lagos Island	8.60	0.20	0.67	0.34	0.16	1.48	0.67	0.59	1.02	0.78	0.52	1.69	1.09
Lagos Mainland	19.31	0.15	0.77	0.30	0.13	1.37	0.63	0.56	1.10	0.78	0.51	1.69	1.07
Mushin	17.32	0.14	0.76	0.34	0.20	1.46	0.71	0.69	1.05	0.84	1.27	1.61	1.34
Ojo	156.70	0.29	0.78	0.41	0.02	1.39	0.54	0.56	1.31	0.76	0.36	1.61	0.96
Oshodi/Isolo	44.39	0.14	0.65	0.31	0.13	1.76	0.62	0.69	1.15	0.81	0.50	1.68	1.32
Shomolu	11.46	0.15	0.50	0.31	0.12	1.11	0.69	0.57	0.94	0.82	0.52	1.69	1.30
Surulere	22.83	0.18	0.61	0.33	0.29	1.89	0.74	0.67	1.12	0.85	0.54	1.67	1.32

**Fig. 7** Variation in mean AOT across 17 LGAs in the Lagos megacity

highest in Ajeromi/Ifeodun and lowest in Eti-Osa with 0.86 and 0.75, respectively. LGAs with a mean AOT higher than or equal to 0.8 include Ikeja, Mushin, Oshodi, Shomolu, and Surulere. In 2020, the overall mean AOT value over all the LGAs was higher than usual, with the highest observed in Ifako/Ijaye, which is slightly higher than the values in Agege, Ajeromi-Ifeodun, Ikeja, Mushin, Oshodi, Shomolu, and Surulere; all within the range of 1.30–1.37. Generally, there are high mean AOT zones in the central region and the south-eastern region of Eti-Osa LGA, except in 2020, where

the high mean AOT is seen in the western and southern parts of the megacity.

Figure 7 shows that the mean AOT for all the LGAs increased in a similar pattern for the study period. The mean distribution of AOT increased progressively from 2002 to 2020 in the different LGAs. Year 2020 has the highest AOT level recorded within the 4 years, while 2002 has the lowest. This variation in the AOT level indicates increased urban activities within these LGAs, leading to air pollutants emissions.

Generally, the AOT distribution over Lagos is observed to have an increasing trend over the years. The concentration is higher at the center (Oshodi, Mushin, Shomolu, Surulere, and Lagos Mainland) for all years except for 2002. This is inferred to result from the increasing urbanization and high commercial activities. Akinyoola et al. (2018) reported that the aerosol loading/concentration is of high increase in the south-south and south-western (coastal) regions of Nigeria, which corroborates the generally high aerosol concentration observed in our findings.

Figure 8 shows the mean AOT per square kilometer. It is observed that the mean AOT per square kilometer has risen over the years. The high values of mean AOT per square kilometer observed in Shomolu, Ajeromi, Agege, and Lagos Island are inversely correlated with their small land area. Conversely, local governments with large areas were seen to have low mean AOT values. It appears that all the LGAs (Lagos Mainland, Lagos Island, Shomolu, Ajeromi, Surulere, and Mushin) located at the center of the study area except in Agege have had a trend of high mean AOT per square kilometer over the years. These high values at the center coincided with the high urbanization density. Meanwhile, the low values observed in Ikorodu, Kosofe, Amuwo Odofin, Eti-Osa, and Alimosho are because the areas are

mixed with built-up areas and vegetation cover and are also located at the edges of the study area in the north, west, and south regions.

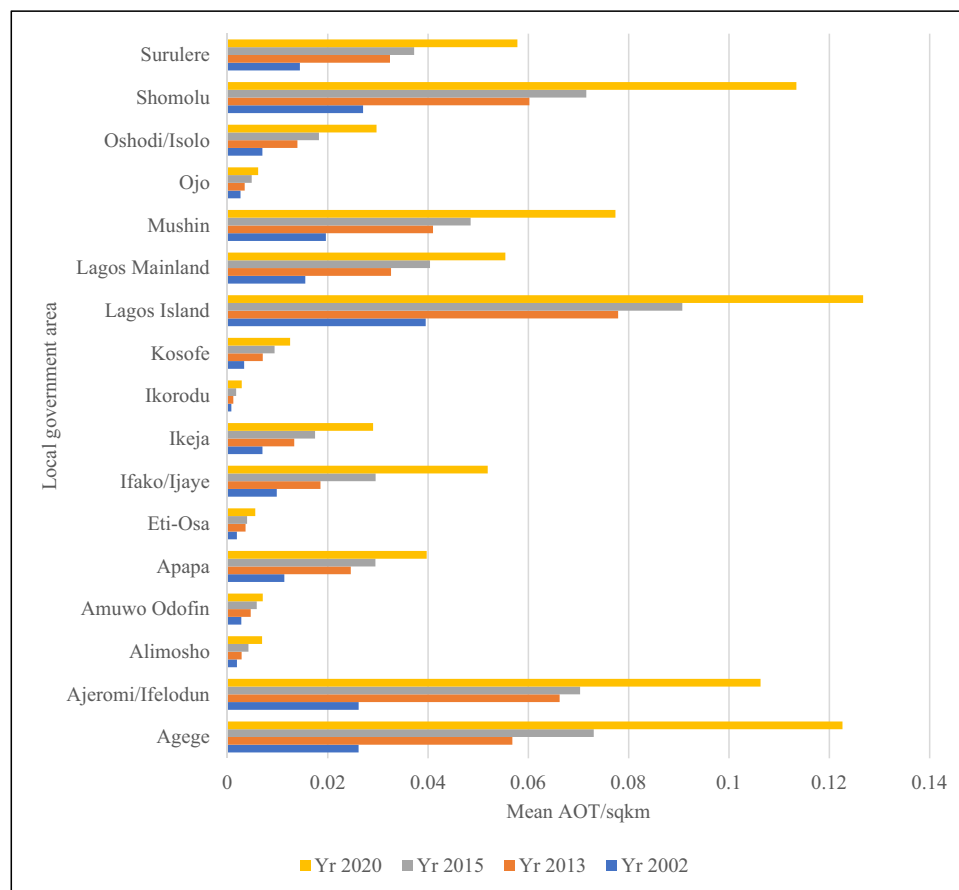
### Correlation of Landsat-derived AOT with in situ PM data

Table 5 presents the correlation between ground-based sample PM data (2019) and imagery-derived AOT (2020) concentrations at both locations. There is a weak positive correlation

**Table 5** Correlation coefficients of the relationship between in situ PM data and imagery-derived AOT for year 2020

Location	PM <sub>1.0</sub>	PM <sub>2.5</sub>	PM <sub>10</sub>	AOT
Onike	PM <sub>1.0</sub>	1.00	0.99	0.99
	PM <sub>2.5</sub>	0.99	1.00	0.99
	PM <sub>10</sub>	0.99	0.99	1.00
	AOT	0.26	0.28	0.29
Okobaba	PM <sub>1.0</sub>	1.00	0.99	0.98
	PM <sub>2.5</sub>	0.99	1.00	0.99
	PM <sub>10</sub>	0.99	0.99	1.00
	AOT	0.70	0.73	0.73

**Fig. 8** Mean AOT per square kilometer



between AOT and  $PM_{1.0}$ ,  $PM_{2.5}$ , and  $PM_{10}$  at Onike, but the correlation between  $PM_{2.5}$  and  $PM_{1.0}$ ,  $PM_{10}$  and  $PM_{1.0}$ , and between  $PM_{10}$  and  $PM_{2.5}$  is quite strong. Okobaba has a strong positive correlation between AOT and  $PM_{1.0}$ , and between  $PM_{2.5}$  and  $PM_{10}$ . There is also a strong positive correlation between  $PM_{2.5}$  and  $PM_{1.0}$ ,  $PM_{10}$  and  $PM_{1.0}$ , and between  $PM_{10}$  and  $PM_{2.5}$ . The values showing the correlation between AOT and PM in Onike are positive but lower than those at Okobaba. The varied correlations could result from the unstable condition of the atmospheric aerosols in coastal environments (Sun et al. 2016). Such dynamics could result in the weak correlation observed at Onike.

## Relationship between AOT and land cover

Figure 9 (a), (b), and (c) show the land cover maps for 2002, 2013, and 2020 respectively, while Table 6 presents the areal distribution of land cover. The trend of built-up area expansion between 2002 and 2020 from the center of the megacity outwards is visible. From a 27.82% coverage in 2002, the built-up areas increased in coverage to approximately 51.89% in 2020. The decline in the coverage area of the vegetation cover is also observed in the study area over the years, resulting in a reduction from 31.92% in 2002 to 12.02% in 2020. This evinces the effects of urbanization on green infrastructure in alleviating air

**Fig. 9** Spatial variation of land cover. (a) 2002. (b) 2013. (c) 2020

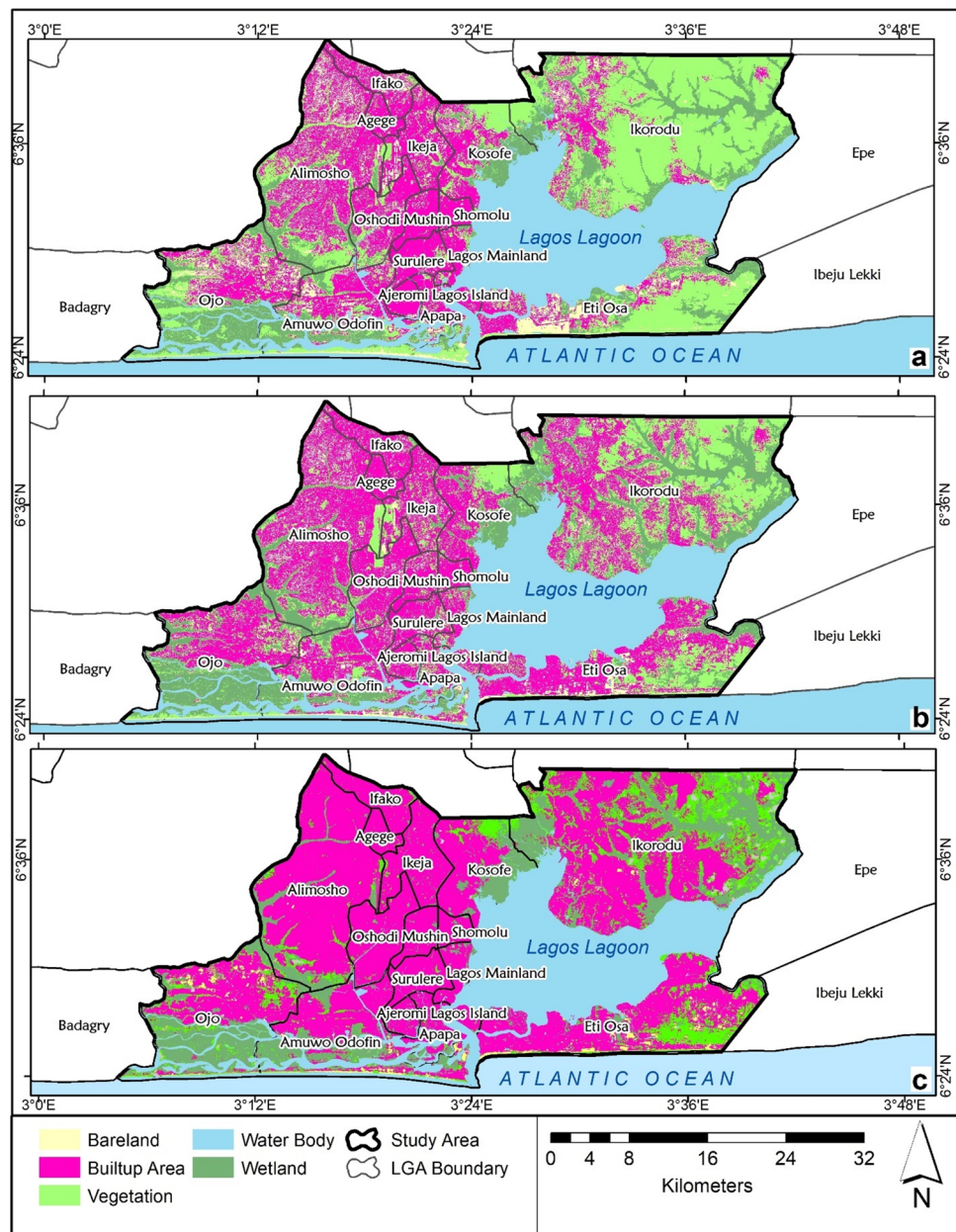


**Table 6** Areal distribution of land cover

Land cover class	Area–2002		Area–2013		Area–2020	
	km <sup>2</sup>	%	km <sup>2</sup>	%	km <sup>2</sup>	%
Bare land	118.46	7.57	96.23	6.15	24.56	1.58
Built-up area	435.10	27.82	592.26	37.86	807.24	51.89
Vegetation	499.21	31.92	336.39	21.51	187.01	12.02
Water body	303.32	19.39	296.43	18.95	284.09	18.26
Wetland	208.08	13.30	242.93	15.53	252.65	16.24

pollution. Notably, the wetland, consisting of mangroves and swamps, increased from 13.3 to 16.24% area coverage between 2002 and 2020. However, there was an increase in 2013 and 2020. The water body coverage has been fairly the same over the years; however, there was a slight decrease between 2002 and 2020 from approximately 19.39 to 18.26% areal coverage. The bare land experienced a drastic reduction from 7.57% areal coverage in 2002 to about 1.58% in 2020.

The distribution of AOT over different land cover types was examined and is presented in Table 7, while a breakdown of the AOT variation for each land cover class is presented in Tables 8, 9, 10, and 11. The areal coverage of bare land declined from 118.46 km<sup>2</sup> in 2002 to 24.56 km<sup>2</sup> in 2020, while its mean AOT exhibited an inverse trend with an increase from 0.4 to 1.25. Generally, the areal coverage of the built-up areas increased over the years, from 435.10 km<sup>2</sup> in 2002 to 807.24 km<sup>2</sup> in 2020. Within the same period (2002 to 2020), the mean AOT increased from 0.35 to 1.32 over built-up areas. The area coverage of vegetation cover declined from 499.21 to 187.01 km<sup>2</sup>, while its mean AOT increased from 0.33 to 1.03 between 2002 and 2020. The mean AOT over wetland areas also increased from 0.32 to 0.73; its areal coverage exhibited an undulating pattern but an overall increase between 2002 and 2020. Generally, it was observed that the highest increase in mean AOT occurred between 2013 and 2020 in bare land, vegetation, and built-up areas. Notably, as

shown in Figs. 6 and 9, the increase in AOT observed in Ikorodu LGA, can be linked with the increase in the built-up areas. A similar trend was observed in the southern edges along with Amuwo Odofin LGA. Overall, the spatial pattern of increase in AOT between 2002 and 2020 is identical to the urban growth through increased built-up areas and decreased vegetation cover. These factors must be considered in future planning and developmental projects to ensure the environment and human health are protected.

The land cover classification results clearly showed that the study area had undergone tremendous spatial changes in its land cover. The observed changes in the land cover are corroborated by the findings of Obiefuna et al. (2021a,b) where an increase in the built-up area, decrease in bare land, and decrease in vegetation cover were observed between 2001 and 2019 in Lagos. Recently, Faisal et al. (2021) reported similar results in their study on the analysis of urban growth and land cover change in Lagos. Their study observed a decline in vegetation coverage, bare land, and water body and an increase in the built-up area between 1990 and 2020. Similarly, Alademomi et al. (2022) assessed land cover change in Amuwo-Odofin LGA within the Lagos megacity and observed that from 2002 to 2019, the highest land cover transitions recorded were from bare land and vegetation to built-up area. All these studies affirm the ongoing accelerated urbanization in Lagos and its detrimental impact on air quality. The land

**Table 7** AOT distribution per land cover class

Class	Year	Count	Area (km <sup>2</sup> )	Min	Max	Range	Mean	SD
Bare land	2002	131,625	118	0.11	0.98	0.86	0.40	0.09
	2013	106,924	96	0.09	1.92	1.83	0.61	0.21
	2020	27,294	25	0.37	1.70	1.34	1.25	0.26
Built-up area	2002	483,444	435	0.05	0.60	0.54	0.35	0.07
	2013	658,064	592	0.06	1.60	1.55	0.63	0.16
	2020	896,934	807	0.37	1.75	1.38	1.32	0.14
Vegetation	2002	554,683	499	0.07	0.80	0.73	0.33	0.06
	2013	373,768	336	0.01	1.62	1.61	0.51	0.14
	2020	207,787	187	0.37	1.68	1.32	1.03	0.35
Wetland	2002	231,202	208	0.08	0.48	0.40	0.32	0.06
	2013	269,917	243	0.03	0.95	0.92	0.56	0.11
	2020	280,720	253	0.36	1.66	1.30	0.73	0.36

**Table 8** Mean AOT distribution in built-up area class per local government area

LGA	2002			2013			2020		
	Area (km <sup>2</sup> )	Area (%)	AOT	Area (km <sup>2</sup> )	Area (%)	AOT	Area (km <sup>2</sup> )	Area (%)	AOT
Agege	9.82	2.26	0.29	10.20	1.72	0.63	10.72	1.33	1.17
Ajeromi	10.77	2.48	0.31	8.82	1.49	0.83	10.62	1.32	1.11
Alimosho	91.22	20.96	0.36	108.06	18.25	0.51	150.71	18.67	1.16
Amuwo Odofin	32.14	7.39	0.39	43.73	7.38	0.73	55.94	6.93	1.08
Apapa	11.30	2.60	0.33	10.42	1.76	0.80	13.81	1.71	1.11
Eti Osa	35.64	8.19	0.38	83.33	14.07	0.80	110.17	13.65	1.07
Ifako	18.13	4.17	0.26	21.02	3.55	0.50	25.07	3.11	1.19
Ikeja	31.95	7.34	0.32	29.00	4.90	0.64	42.64	5.28	1.15
Ikorodu	42.06	9.67	0.31	112.65	19.02	0.50	178.43	22.10	1.13
Kosofe	26.97	6.20	0.32	29.85	5.04	0.65	39.44	4.89	1.11
Lagos Island	4.71	1.08	0.38	3.81	0.64	0.83	5.36	0.66	1.13
Lagos Mainland	9.71	2.23	0.33	8.46	1.43	0.76	11.94	1.48	1.09
Mushin	15.84	3.64	0.33	13.76	2.32	0.72	16.42	2.03	1.14
Ojo	36.33	8.35	0.44	49.04	8.28	0.60	60.39	7.48	1.12
Oshodi	29.01	6.67	0.32	33.16	5.60	0.63	42.30	5.24	1.13
Shomolu	9.62	2.21	0.32	9.14	1.54	0.73	10.74	1.33	1.15
Surulere	19.89	4.57	0.33	17.80	3.01	0.76	22.56	2.79	1.12

**Table 9** Mean AOT distribution in vegetation class per local government area

LGA	2002			2013			2020		
	Area (km <sup>2</sup> )	Area (%)	AOT	Area (km <sup>2</sup> )	Area (%)	AOT	Area (km <sup>2</sup> )	Area (%)	AOT
Agege	0.82	0.16	0.29	0.46	0.14	0.56	0.32	0.17	1.12
Ajeromi	0.80	0.16	0.33	2.78	0.83	0.77	0.13	0.07	1.20
Alimosho	44.88	8.98	0.34	23.63	7.02	0.53	10.52	5.63	0.79
Amuwo Odofin	37.96	7.59	0.36	27.10	8.05	0.60	14.02	7.50	0.66
Apapa	5.09	1.02	0.30	5.64	1.67	0.71	0.87	0.47	0.75
Eti Osa	79.21	15.84	0.34	52.26	15.53	0.62	34.84	18.64	0.49
Ifako	3.58	0.72	0.24	2.03	0.60	0.45	0.99	0.53	1.07
Ikeja	8.28	1.66	0.29	11.33	3.37	0.56	1.25	0.67	1.03
Ikorodu	238.11	47.63	0.32	145.28	43.18	0.42	91.83	49.12	0.99
Kosofe	22.18	4.44	0.27	18.03	5.36	0.52	7.94	4.25	0.93
Lagos Island	0.67	0.13	0.34	1.73	0.51	0.77	0.09	0.05	1.02
Lagos Mainland	3.34	0.67	0.28	4.11	1.22	0.69	0.12	0.06	0.90
Mushin	0.73	0.15	0.34	2.39	0.71	0.65	0.00	0.00	0.00
Ojo	42.19	8.44	0.40	28.85	8.58	0.51	22.94	12.27	0.76
Oshodi	9.34	1.87	0.29	6.22	1.85	0.58	0.80	0.43	0.99
Shomolu	0.56	0.11	0.28	1.02	0.30	0.64	0.06	0.03	0.88
Surulere	2.18	0.44	0.30	3.62	1.07	0.68	0.21	0.11	0.84

cover distribution influences the aerosol concentration. The mean AOT in the built-up area showed an increasing trend from 2002 to 2020, as shown in Table 8. Moreover, it has been widely established that factors such as population expansion and accelerated urban growth are significant contributors to air pollution. The wetlands also showed a high AOT with a range of 0.00–0.35, 0.00–0.67, and

0.43–1.13 for 2002, 2013, and 2020 respectively. However, there is a clear distinction in the distribution of AOT in urban areas compared to wetlands. As shown in Table 11, the lowest mean wetland AOTs for 2002, 2013, and 2020 are 0.00, 0.00, and 0.43, respectively, contradicting that of the built-up areas. However, further studies are required to understand the seasonal variations in the mean AOTs

**Table 10** Mean AOT distribution in bare land class per local government area

LGA	2002			2013			2020		
	Area (km <sup>2</sup> )	Area (%)	AOT	Area (km <sup>2</sup> )	Area (%)	AOT	Area (km <sup>2</sup> )	Area (%)	AOT
Agege	0.46	0.39	0.31	0.44	0.46	0.59	0.00	0.00	0.00
Ajeromi	0.40	0.33	0.40	0.36	0.37	0.80	0.00	0.00	0.00
Alimosho	28.48	24.09	0.36	27.87	28.99	0.49	0.32	1.41	1.02
Amuwo Odofin	13.23	11.20	0.43	10.43	10.84	0.69	4.99	21.64	1.03
Apapa	1.11	0.94	0.36	0.65	0.68	0.85	0.05	0.21	0.60
Eti Osa	24.52	20.75	0.47	15.68	16.30	0.90	10.43	45.29	1.05
Ifako	4.44	3.76	0.28	2.81	2.92	0.48	0.00	0.00	0.00
Ikeja	5.27	4.46	0.34	4.48	4.66	0.62	0.00	0.00	0.00
Ikorodu	13.61	11.52	0.34	17.02	17.70	0.50	1.44	6.24	1.12
Kosofe	3.24	2.74	0.34	1.82	1.89	0.63	0.04	0.18	1.09
Lagos Island	0.14	0.12	0.41	0.34	0.35	0.73	0.00	0.02	1.16
Lagos Mainland	0.53	0.45	0.36	0.52	0.54	0.71	0.01	0.06	0.97
Mushin	0.75	0.63	0.40	1.18	1.22	0.69	0.00	0.00	0.00
Ojo	16.92	14.31	0.46	7.25	7.54	0.54	5.75	24.96	1.06
Oshodi	4.05	3.42	0.34	3.90	4.05	0.62	0.00	0.00	0.00
Shomolu	0.38	0.32	0.33	0.37	0.39	0.63	0.00	0.00	0.00
Surulere	0.67	0.57	0.41	1.04	1.08	0.79	0.00	0.00	0.00

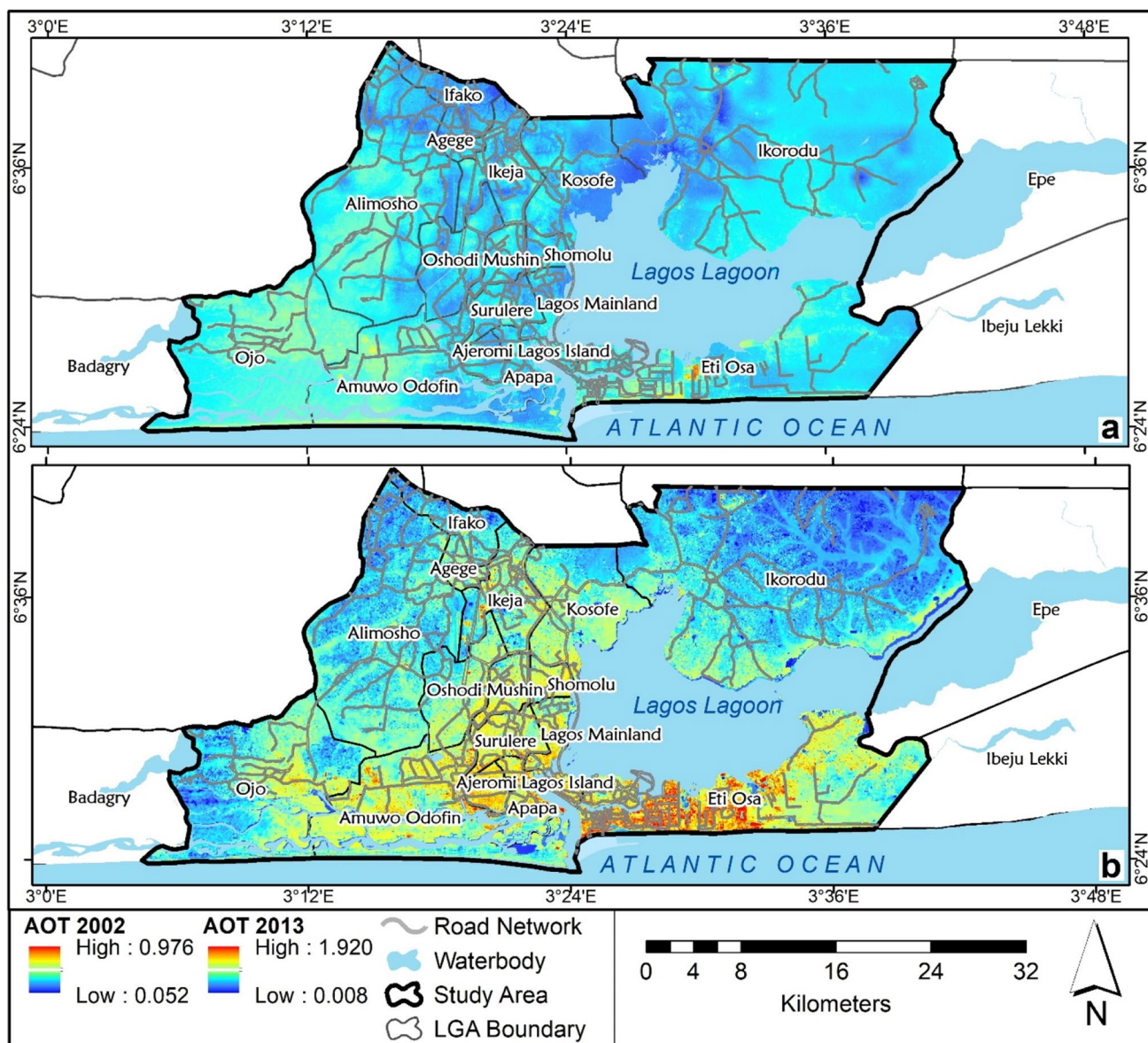
**Table 11** Mean AOT distribution in wetland class per local government area

LGA	2002			2013			2020		
	Area (km <sup>2</sup> )	Area (%)	AOT	Area (km <sup>2</sup> )	Area (%)	AOT	Area (km <sup>2</sup> )	Area (%)	AOT
Agege	0.00	0.00	0.00	0.00	0.00	0.00	0.06	0.03	1.13
Ajeromi	0.00	0.00	0.00	0.00	0.00	0.00	1.22	0.48	1.09
Alimosho	18.96	9.12	0.34	24.00	14.23	0.58	21.60	8.58	0.57
Amuwo Odofin	25.87	12.45	0.35	12.90	7.65	0.67	35.71	14.19	0.45
Apapa	1.52	0.73	0.25	0.60	0.35	0.64	4.24	1.68	0.69
Eti Osa	24.77	11.91	0.32	9.64	5.72	0.62	12.67	5.03	0.69
Ifako	0.26	0.12	0.14	0.53	0.32	0.47	0.31	0.12	0.85
Ikeja	0.27	0.13	0.26	0.96	0.57	0.56	1.79	0.71	1.08
Ikorodu	69.19	33.28	0.30	73.61	43.65	0.48	88.88	35.31	0.55
Kosofe	16.52	7.95	0.22	9.86	5.85	0.58	23.74	9.43	0.46
Lagos Island	0.00	0.00	0.00	0.00	0.00	0.00	0.49	0.19	0.96
Lagos Mainland	0.87	0.42	0.25	0.52	0.31	0.60	2.87	1.14	0.74
Mushin	0.00	0.00	0.00	0.00	0.00	0.00	0.90	0.36	1.13
Ojo	47.77	22.98	0.38	34.53	20.48	0.53	54.36	21.60	0.43
Oshodi	1.79	0.86	0.27	1.04	0.62	0.58	1.24	0.49	1.04
Shomolu	0.01	0.01	0.24	0.06	0.03	0.57	1.16	0.46	0.99
Surulere	0.09	0.04	0.23	0.37	0.22	0.60	0.46	0.18	1.09

### Relationship between AOT and road network distribution

Figure 10 (a), (b), (c), and (d) show the overlay of 60-m major road buffer zones on the AOT maps for 2002, 2013, 2015, and 2020 respectively. Due to the low spatial variability of aerosols over a small area, a road buffer of 60 m

was used to examine the concentration of AOT along the road network. From the results, it was observed that the AOT concentration was higher along the major roads. This can be attributed to the high level of air pollutants emitted from vehicles, including home/office generators and industries located along the road corridors. From Table 12, the mean AOT along road network (ARN) is higher than that

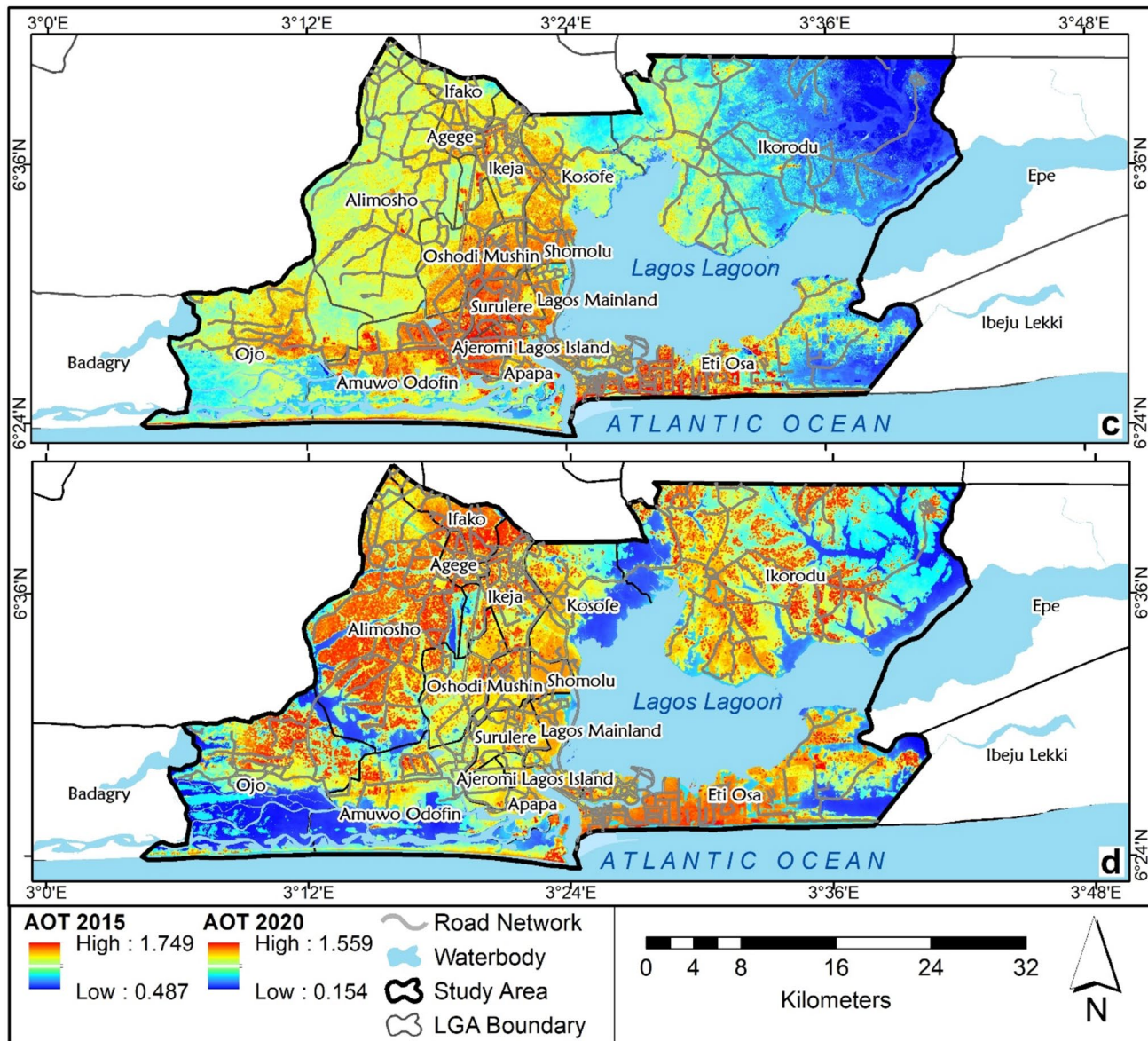


**Fig. 10** Overlay of 60-m major road buffers on AOT maps. (a) 2002. (b) 2013. (c) 2015 (d) 2020

observed outside road network (ORN) for all years. This is corroborated by the AOT maps, which show that the AOT concentration is higher along the major roads, especially in the center of the megacity and over Eti-Osa region except for the year 2002. The high AOT in these regions can be attributed to the high daily traffic experienced in the highly urbanized megacity. The lowest AOT is 0.01 (ORN), while the highest is 1.92 (ORN). Table 13 presents the correlation between road network density and mean AOT.

The persistent vehicular traffic congestion, population congestion, and industrial and commercial activities in Lagos State (see Figs. 11 and 12) lead to increased pollutant

emissions and a deleterious impact on residents' well-being. It was observed that the AOT concentration is higher along the road corridors. This agrees with the findings of Adeyanju and Manohar (2017) in their study on the effects of vehicular emissions on environmental pollution in Lagos. In their study, they observed a decreasing concentration of pollutants with increasing distance from traffic routes. According to UNEP (2016), Nigeria is one of the countries that have made major investments in public transport in the last 5 years. However, there are no advanced vehicle emission standards. Miller (2019) posited that on-road diesel vehicles were one of Nigeria's most significant contributors to poor health in

**Fig. 10** (continued)**Table 12** Concentration of AOT on road corridors

	Year	Region	Area (km <sup>2</sup> )	AOT				
				Min	Max	Range	Mean	SD
2002	ARN	114	0.07	0.92	0.85	0.35	0.07	
	ORN	1451	0.05	0.98	0.92	0.33	0.07	
2013	ARN	114	0.09	1.74	1.66	0.66	0.18	
	ORN	1451	0.01	1.92	1.91	0.53	0.17	
2015	ARN	114	0.54	1.24	0.70	0.80	0.06	
	ORN	1451	0.49	1.75	1.26	0.73	0.07	
2020	ARN	114	0.43	1.71	1.28	1.31	0.15	
	ORN	1451	0.36	1.75	1.39	1.05	0.38	

ARN, along road network; ORN, outside road network

**Table 13** Correlation coefficients between road network density and mean AOT

	Road density	AOT 2002	AOT 2013	AOT 2015	AOT 2020
Road density	1	-0.01	0.37	0.46	0.22
AOT 2002	-0.01	1	0.27	0.25	0.18
AOT 2013	0.37	0.27	1	0.73	0.23
AOT 2015	0.46	0.25	0.73	1	0.41
AOT 2020	0.22	0.18	0.23	0.41	1

**Fig. 11** Commuters and open market along a busy road at Orile in the Lagos megacity

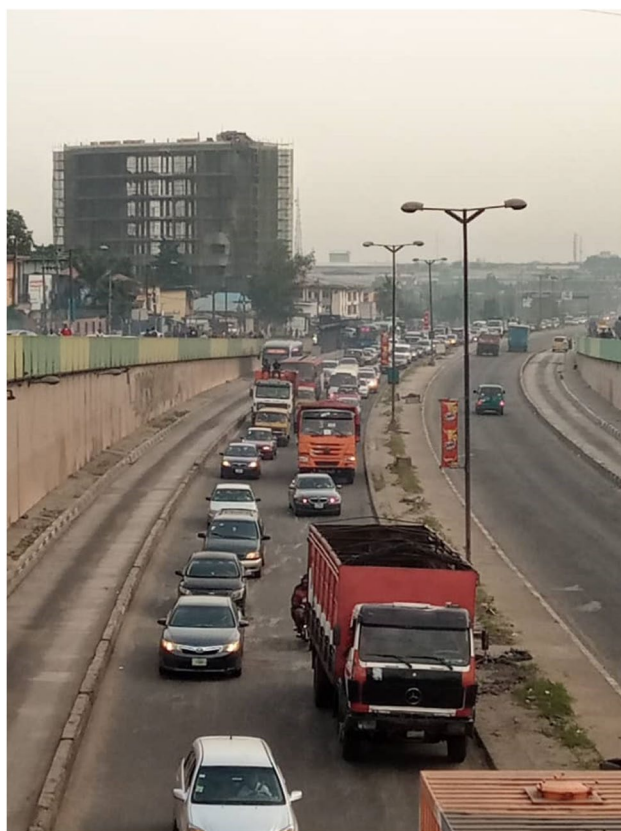


**Fig. 12** Build-up of vehicular traffic at Maryland in the Lagos megacity

2015, including on-road non-diesel vehicles, international shipping, and non-road mobile sources.

## Conclusion and recommendations

This study only examined the air pollution distribution during the dry season. Studies have shown that air pollution is higher in the dry season than in the wet season, during which dust-laden north-easterly trade winds blow in from the Sahara Desert. The increased AOT observed in the megacity is an indication of increased urbanization, including industrial and traffic activities. The relationship between AOT and the different particulate matter sizes showed similar correlation coefficient values with a weak positive correlation at Onike, and a strong positive correlation at Okobaba. Additional ground-based data could have enabled a more extensive validation. Also, this study only considered the dry season. The problem of cloud cover on wet season Landsat imageries is a limitation on the potential to evaluate the seasonal variations in AOT.

Full-scale monitoring of air pollution over the whole of Lagos State should be encouraged to inform the government and environmental agencies of this perilous atmospheric situation. Researchers should also adopt satellite-based methods for air quality monitoring over Lagos State.

The high AOT concentration observed in the megacity should necessitate the government's establishment of Ambient

Air Quality Standards (AAQS). Air quality monitoring and modelling, in addition to the provision of AAQS, are significant instruments for air quality management. However, most countries only monitor air quality on a sporadic basis, if at all. Because air quality data are scarce, evaluating the potential air quality impacts on a country from multiple sources is challenging. As a result, the government should consider the establishment of multiple air quality monitoring stations to acquire real-time air quality information. The government should consider exploring clean mobility by creating national electric mobility strategies to reduce vehicular emissions. In addition, government should enforce proper city planning to manage the urbanization growth in the megacity.

The environmental agencies could use the findings from this study to make informed decisions on how to control environmental air pollution. Information concerning the concentration and variability could help decide where to set up air pollution monitoring stations. With a view to making cities and human settlements inclusive, safe, resilient, and sustainable, this study contributes to the United Nations Sustainable Development Goals (SDGs) number 11, specifically goal 11.6, which aims to reduce the adverse per capita environmental impact of cities. The rapid growth of the Lagos megacity and its projected increase justifies the need to study the state's dynamics and futuristic outlook on air quality.

**Acknowledgements** The authors would like to thank the NASA/USGS for free access to Landsat imageries and the Air Quality Monitoring Group (AQM) Unilag for providing the ground-based PM data. The authors also commend Jorge Vicent Servera for their support in using the Py6S model.

**Author contribution** Emmanuel Ayodele, Conceptualization, writing—review and editing, supervision, project administration.

Chukwuma Okolie, Conceptualization, validation, formal analysis, writing—review and editing, visualization, supervision

Samuel Akinnusi, Conceptualization, methodology, software, formal analysis, validation, investigation, data curation, writing—original draft, review and editing, visualization

Erom Mbu-Ogar, Methodology, software, formal analysis, validation, investigation, writing—original draft, visualization

Rose Alani, Resources, data curation, writing—review and editing

Olagoke Daramola, Conceptualization, methodology, software, supervision

Abdulwaheed Tella, Methodology, investigation, writing—review and editing

**Data Availability** The datasets generated and analyzed during the current study are available from the corresponding author on reasonable request.

## Declarations

**Ethical approval** Not applicable

**Consent to participate** Not applicable

**Consent for publication** Not applicable

**Competing interests** The authors declare no competing interests.

## References

- Adeyanju AA, Manohar K (2017) Effects of vehicular emission on environmental pollution in Lagos. *Sci-Afric J Sci Issues Res Essays* 5(4):34–51
- Adeyewa ZD, Oluleye A (2011) International journal of remote relationships between aerosol index, ozone, solar zenith angle and surface reflectivity : a case study of satellite observations over Lagos. *Int J Remote Sens* 37:41. <https://doi.org/10.1080/01431161003705883>
- Akinyoola JA, Eresanya EO, Orimoogunje OOI, Oladosu K (2018) Monitoring the spatio-temporal aerosol loading over Nigeria. *Model Earth Syst Environ* 4(4):1365–1375. <https://doi.org/10.1007/s40808-018-0485-2>
- Alademomi AS, Okolie CJ, Daramola OE, Agboola RO, Salami TJ (2020) Assessing the relationship of LST, NDVI and EVI with land cover changes in the Lagos Lagoon environment. *Quaestiones Geographicae* 39(3):87–109. <https://doi.org/10.2478/quageo-2020-0025>
- Alademomi AS, Okolie CJ, Daramola OE, Akinnusi SA, Adediran E, Olanrewaju HO, Alabi AO, Salami TJ, Odumosu J (2022) The interrelationship between LST, NDVI, NDBI, and land cover change in a section of Lagos metropolis, Nigeria. *Appl Geomat* 14:299–314. <https://doi.org/10.1007/s12518-022-00434-2>
- Alani RA, Ayejuyo OO, Akinrinade OE et al (2019) The level PM2.5 and the elemental compositions of some potential receptor locations in Lagos, Nigeria. *Air Qual Atmos Health* 12:1251–1258. <https://doi.org/10.1007/s11869-019-00743-3>
- Anderson JR (1971) Land use classification schemes used in selected recent geographic applications of remote sensing. *Photogrammetric Engineering* 37(4):379–387
- Car Mart (2022). Lagos state vehicle registration and plate number verification. <https://www.carmart.ng/public/blog/lagos-state-vehicle-registration-and-plate-number-verification/> (Date accessed: 10th June, 2022)
- CNN Travel (2019). Marketplace Africa: employees in Lagos are stressed, burned out and exhausted because of ‘hellish traffic’. <https://edition.cnn.com/travel/article/traffic-stress-lagos-niger-ia/index.html> (Date accessed: 30 July 2021)
- Das S, Angadi DP (2020) Land use-land cover (LULC) transformation and its relation with land surface temperature changes: a case study of Barrackpore Subdivision, West Bengal, India. *Remote Sensing Applications: Society and Environment* 19(May):100322. <https://doi.org/10.1016/j.rsase.2020.100322>
- Deuzé JL et al (2001) Remote sensing of aerosols over land surfaces from POLDER-ADEOS-1 polarized measurements. *J Geophys Res* 106(D5):4913–4926. <https://doi.org/10.1029/2000JD900364>
- Ding H, Shi J, Wang Y, Wei L (2015) An improved dark-object subtraction method for atmospheric correction of Landsat 8. *Proc of SPIE* 9815:1–8. <https://doi.org/10.1117/12.2205567>
- Faisal KA, Yue W, Abdullahi AG, Hamed R, Noman AAA (2021) Analyzing urban growth and land cover change scenario in Lagos, Nigeria using multi-temporal remote sensing data and GIS to mitigate flooding. *Geomat Nat Haz Risk* 12(1):631–652. <https://doi.org/10.1080/19475705.2021.1887940>
- Herman JR, Bhartia PK, Torres O, Hsu C, Sefor C, Celarier E (1997) Global distribution of UV-absorbing aerosols from Nimbus 7/TOMS data. *J Geophys Res Atmos* 102(14):16911–16922. <https://doi.org/10.1029/96jd03680>
- Holben BN et al (1998) AERONET-A federated instrument network and data archive for aerosol characterization. *Remote Sens Environ* 66:1–16
- Joshi J, Kandpal KC, Rawat N (2019) Estimation of air pollution using multi-temporal remote sensing technique for Dehradun District, Uttarakhand. *Int J Adv Remote Sens GIS* 8(1):2919–2932. <https://doi.org/10.23953/cloud.ijarsg.400>

- Kaufman YJ, Sendra C (1988) Algorithm for automatic atmospheric corrections to visible and near-ir satellite imagery. *Int J Remote Sens* 9(8):1357–1381. <https://doi.org/10.1080/01431168808954942>
- Kaufman YJ, Tanré D, Gordon HR, Nakajima T, Lenoble J, Frouin R, Grassl H, Herman BM, King MD, Teillet PM (1997) Passive remote sensing of tropospheric aerosol and atmospheric correction for the aerosol effect. *J Geophys Res Atmos* 102(14):16815–16830. <https://doi.org/10.1029/97jd01496>
- L3Harris Geospatial (2021) Software & Technology ENVI. <https://www.l3harrisgeospatial.com/Software-Technology/ENVI> (Date accessed: 30 July 2021)
- Levy RC, Remer LA, Kleidman RG, Mattoo S, Ichoku C, Kahn R, Eck TF (2010) Global evaluation of the Collection 5 MODIS dark-target aerosol products over land. *Atmos Chem Phys* 10(21):10399–10420. <https://doi.org/10.5194/acp-10-10399-2010>
- Levy RC, Remer LA, Mattoo S, Vermote EF, Kaufman YJ (2007) Second-generation operational algorithm: Retrieval of aerosol properties over land from inversion of Moderate Resolution Imaging Spectroradiometer spectral reflectance. *J Geophys Res Atmos* 112(13):1–21. <https://doi.org/10.1029/2006JD007811>
- Liu J, Ding J, Li L, Li X, Zhang Z, Ran S, Ge X, Zhang J, Wang J (2020) Characteristics of aerosol optical depth over land types in central Asia. *Sci Total Environ* 727:138676. <https://doi.org/10.1016/j.scitotenv.2020.138676>
- Luo N, Sing M, Zhao W, Yan X, Xiao F (2015) Improved aerosol retrieval algorithm using Landsat images and its application for PM 10 monitoring over urban areas. *Atmos Res* 153:264–275. <https://doi.org/10.1016/j.atmosres.2014.08.012>
- Mayer B, Kylling A (2005) Technical note: the libRadtran software package for radiative transfer calculations - Description and examples of use. *Atmos Chem Phys* 5(7):1855–1877. <https://doi.org/10.5194/acp-5-1855-2005>
- Miller J (2019) Costs and benefits of soot-free road transport in Nigeria (Issue August). [https://theicct.org/sites/default/files/publications/ICCT\\_Sootfree\\_transport\\_20190826.pdf%0A https://trid.trb.org/view/1649938](https://theicct.org/sites/default/files/publications/ICCT_Sootfree_transport_20190826.pdf%0A https://trid.trb.org/view/1649938)
- Mogaji E (2020) Impact of COVID-19 on transportation in Lagos, Nigeria. *Transp Res Interdiscip Perspect* 6 <https://doi.org/10.1016/j.trip.2020.100154>
- Njoku LK, Rumide JT, Akinola MO, Adesuyi AA, Jolaoso AO (2016) Ambient air quality monitoring in Metropolitan City of Lagos, Nigeria. *J Appl Sci Environ Manag* 20(1):178–185. <https://doi.org/10.4314/jasem.v20i1.21>
- Obiefuna JN, Nwilo PC, Atagbaza AO, Okolie CJ (2013) Spatial changes in the wetlands of Lagos/Lekki lagoons of Lagos, Nigeria. *J Sustain Dev* 6(7):123–133. <https://doi.org/10.5539/jsd.v6n7p123>
- Obiefuna JN, Okolie CJ, Atagbaza AO, Nwilo PC, Akindeju FO (2021a) Spatio-temporal land cover dynamics and emerging landscape patterns in western part of Lagos State, Nigeria. *Environ Socio-Econ Stud* 9(3):53–69. <https://doi.org/10.2478/envion-2021-0017>
- Obiefuna JN, Okolie CJ, Nwilo PC, Daramola OE, Isiofia L (2021b) Potential influence of urban sprawl and changing land surface temperature on outdoor thermal comfort in Lagos State, Nigeria. *Quaest Geogr* 40(1):5–23. <https://doi.org/10.2478/quageo-2021-0001>
- Oguntunde PE, Odetunmibi OA, Adejumo AO (2014) A study of probability models in monitoring environmental pollution in Nigeria. *J Probab Stat*
- Okolie CJ, Ayodele EG, Mbu-Ogar E, Akinnusi SA, Daramola OE, Tella A, Alani RA, Alademomi AS (2021) Remote sensing approach for aerosol optical thickness (AOT) monitoring in relation to the road network in Lagos Metropolis, Nigeria. In: Proceedings of the 3rd Intercontinental Geoinformation Days (IGD) Conference, Mersin University, Turkey, 17th – 18th November 2021
- Olowoporoku AO, Longhurst JWS, Barnes JH (2012) Framing air pollution as a major health risk in Lagos, Nigeria. *WIT Trans Ecol Environ* 157:479–486. <https://doi.org/10.2495/AIR120421>
- Oluyemi EA, Asubiojo OI (2001) Ambient air particulate matter in Lagos, Nigeria. *Bull Chem Soc Ethiop* 15(2):97–108
- Omari K, Abuelgasim A, Alhebsi K (2019) Aerosol optical depth retrieval over the city of Abu Dhabi, United Arab Emirates ( UAE ) using Landsat-8 OLI images. *Atmos Pollut Res* 10(4):1075–1083. <https://doi.org/10.1016/j.apr.2019.01.015>
- Ou Y, Chen F, Zhao W, Yan X, Zhang Q (2017) Landsat 8-based inversion methods for aerosol optical depths in the Beijing area. *Atmos Pollut Res* 8(2):267–274. <https://doi.org/10.1016/j.apr.2016.09.004>
- Prakash BM, Mahadevaswamy M, Mahesh S, Vishala, N (2016) Prediction of air pollutants dispersion emitted from point and line sources along the highway passing through industrial area of Mysuru- AERMOD and CALINE4 models. *Int J Innov Res Sci Eng Technol* 5(8):14497–14508. <https://doi.org/10.15680/IJRSET.2016.0508027>
- Ranjan AK, Patra AK, Gorai AK (2020) A review on estimation of particulate matter from satellite-based aerosol optical depth: data, methods, and challenges. *Asia Pac J Atmos Sci.* <https://doi.org/10.1007/s13143-020-00215-0>
- Sun L, Wei J, Bilal M, Tian X, Jia C, Guo Y (2016) Aerosol optical depth retrieval over bright areas using Landsat 8 OLI images. *Remote Sens (Basel)* 8(23):1–14. <https://doi.org/10.3390/rs8010023>
- Taiwo AM, Arowolo TA, Abdullahi KL, Taiwo OT (2015) Particulate matter pollution in Nigeria: a review. In: Proceedings of the 14th International Conference on Environmental Science and Technology, September, 3–5
- Tanre D, Deschamps PY, Leffé AD (1979) Atmospheric modelling for space measurements of ground reflectances, including bidirectional properties. *Appl Optics* 18(21)
- Tella A, Abdul-Lateef B, Ibrahima F (2021) Spatio-temporal modeling of the influence of climatic variables and seasonal variation on PM10 in Malaysia using multivariate regression (MVR) and GIS. *Geomat Nat Haz Risk* 12:443–468
- Tian L, Hou W, Chen J, Chen C, Pan X (2018) Spatiotemporal changes in PM2.5 and their relationships with land-use and people in Hangzhou. *Int J Environ Res Public Health* 15(10):1–14. <https://doi.org/10.3390/ijerph15102192>
- UNEP (2016) Actions on air quality: policies & programmes for improving air quality around the world. In: Actions on Air Quality. <https://doi.org/10.18356/9811f020-en>
- Vermote EF, Tanre D, Deuze JL, Herman M, Morcette JJ (1997) Second simulation of the satellite signal in the solar spectrum, 6S: an overview. *IEEE Trans Geosci Remote Sens* 35(3):675–686. <https://doi.org/10.1109/36.581987>
- Wei X, Chang NB, Bai K, Gao W (2020) Satellite remote sensing of aerosol optical depth: advances, challenges, and perspectives. *Crit Rev Environ Sci Technol* 50(16):1640–1725. <https://doi.org/10.1080/10643389.2019.1665944>
- Wilson RT (2013) Py6S: A python interface to the 6s radiative transfer model. *Comput Geosci* 51:166–171. <https://doi.org/10.1016/j.cageo.2012.08.002>
- Yang H, Chen W, Liang Z (2017) Impact of land use on PM 2.5 pollution in a representative city of Middle China. <https://doi.org/10.3390/ijerph14050462>
- Yusuf KA, Oluwole S, Abdusalam IO, Adewusi GR (2013) Spatial patterns of urban air pollution in an industrial estate, Lagos, Nigeria spatial patterns of urban air pollution in an industrial estate, Lagos, Nigeria. *Int J Eng Invent* 2(4):1–9

- Zhang L, Shi R, Liu C, Zhou C (2015) Retrieval of aerosol optical depth over Beijing using Landsat8 / OLI data. Proceedings of SPIE 9610:1–8. <https://doi.org/10.1117/12.2186761>
- Zhang Y, Liu Z, Wang Y, Ye Z, Leng L (2014) Inversion of aerosol optical depth based on the CCD and IRS sensors on the HJ-1 satellites. *Remote Sens (Basel)* 6:8760–8778. <https://doi.org/10.3390/rs6098760>
- Zhao WJ, Ou Y, Chen F, Zhao W, Yan X, Zhang Q (2016) Landsat 8-based inversion methods for aerosol optical depths in the Beijing area atmospheric pollution research Landsat 8-based inversion methods for aerosol optical depths in the Beijing area. *Atmos Pollut Res* 8(2):267–274. <https://doi.org/10.1016/j.apr.2016.09.004>

**Publisher's note** Springer Nature remains neutral with regard to jurisdictional claims in published maps and institutional affiliations.

Springer Nature or its licensor (e.g. a society or other partner) holds exclusive rights to this article under a publishing agreement with the author(s) or other rightsholder(s); author self-archiving of the accepted manuscript version of this article is solely governed by the terms of such publishing agreement and applicable law.